ACS APPLIED NANO MATERIALS

www.acsanm.org Article

Rolled-Up Quantum Wells Composed of Nanolayered InGaAs/GaAs Heterostructures as Optical Materials for Quantum Information Technology

Leonarde N. Rodrigues, Diego Scolfaro, Lucas da Conceição, Angelo Malachias, Odilon D. D. Couto, Jr, Fernando Iikawa, and Christoph Deneke*

Cite This: *ACS Appl. Nano Mater.* 2021, 4, 3140−3147 Read Online

ACCESS | Metrics & More | Article Recommendations

ABSTRACT: Strain-based band structure engineering is a powerful tool to tune the optical and electronic properties of semiconductor nanostructures. We show that we can tune the band structure of InGaAs semiconductor quantum wells and modify the helicity of the emitted light by integrating them into rolled-up heterostructures and changing their geometrical configuration. Experimental results from photoluminescence and photoluminescence excitation spectroscopy demonstrate a strong energy shift of the valence-band states in comparison to flat structures, as a consequence of an inversion of the heavy-hole with the light-hole states in a rolled-up InGaAs quantum well. The inversion and mixing of the band states lead to a strong change in the optical selection rules for the rolled-up quantum wells, which show vanishing spin polarization in the conduction band even under near-resonant excitation conditions. Band structure calculations are carried out to understand the changes in the electronic transitions and to predict the emission and absorption spectra for a given geometrical configuration. Comparison between experiment and theory shows an excellent agreement. These observed profound changes in the fundamental properties can be applied as a strategic route to develop novel optical devices for quantum information technology.

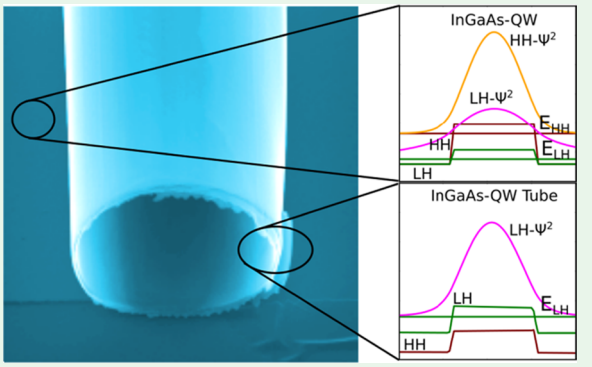

KEYWORDS: *band structure inversion, semiconductor quantum well, optical selection rules, rolled-up microtubes, tensile and compressive hybrid state, curved semiconductor membrane*

INTRODUCTION

Strain engineering of IV and III−V structures is a well-established method to tailor the optical and electronic properties of semiconductors. This includes strained silicon for high-performance central processing units (CPUs),[1] the modification of the optical properties of Ge,[2−4] or the modification of emission properties of III−V devices.[5] In the last years, there is considerable effort to tune the band structure to change the emission properties of nanometric-sized quantum structures integrated into membranes using an external applied strain.[4,6−12] Hereby, tuning of the Ge band gap from indirect to direct has been achieved,[4] emission of two single-photon sources tuned into resonance,[9] or an inversion of the band alignment of quantum emitters has been reported.[7,8] The disadvantage of external application of mechanical stress (for any type of structure)[6−8,10−12] is that the achieved strain is very local (spatially restricted to a submicron range) and requires a constant external control to maintain the applied strain.[12]

Rolled-up semiconductor three-dimensional (3D) architectures based on the deterministic release of strained layers have been explored in the last 2 decades as building blocks in nano- and microtechnologies.[13−20] Their use as optical resonators[21−28] to realize laser structures[28−31] gained particular attention. For this, optical emitters like quantum wells (QWs) and quantum dots have been integrated into the tube walls.[21,28,32−34] Attraction of the method stems from the easy control of basic parameters like tube radius[35] and the possibility to control the position of the formed nano- and micro-objects precisely.[17] It is well known that the resulting strain profile of the tubes influences the optical properties of the embedded emitter.[32−34,36,37] In the past, these structures

Received: February 3, 2021
Accepted: February 12, 2021
Published: February 23, 2021

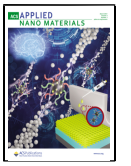

https://dx.doi.org/10.1021/acsanm.1c00354
ACS Appl. Nano Mater. 2021, 4, 3140−3147

have been designed to minimize strain effects, and little advantage of the strain engineering possibility has been taken. On the other hand, strain engineering technology has been used in different nanomembrane semiconductor systems to optimize and control optoelectronic properties. Thereby, a biaxial tensile strain state is provided via external potential, and curved systems such as rolled-up tubes enable a tensile and compressive hybrid state at the same time without external strain.[36,38] The potential to fabricate curved structures with diameters from a few nanometers (e.g., minimum diameter ~10 nm for monolayer-based InAs/GaAs system[35,39]) to several micrometers allows us to modify in a unique way the strain distribution over the tube wall layers, i.e., along the radial tube direction.

Here, we show that we can tune the optical emission characteristics of GaAs and InGaAs, as well as quantum wells (QWs) solely by changing their geometry from a flat to a curved heterostructure without the need to apply an external strain. Specifically, we demonstrate, by comparing the behavior of a (rolled-up) InGaAs quantum well (InGaAs-QW) to a previously investigated (rolled-up) GaAs quantum well (GaAs-QW),[36] the ability to considerably change the optical excitation selection rules of these nanostructures by strain engineering. For this, we carry out micro-photoluminescence (μ-PL) and circularly polarized micro-photoluminescence excitation (μ-PLE) on flat and rolled-up quantum wells. By comparing our experimental results with band structure calculations, we find clear evidence that the absorption energy shift is a consequence of valence-band state mixing and, most importantly, the induction of a fundamental band gap transition involving the light-hole (LH) valence-band states. Such a transition involves mixed wavefunctions with different symmetries compared to the heavy-hole (HH)-state wave function, thus leading to negligible electron spin polarization density excited in the conduction band. X-ray diffraction (XRD) measurements are used as input to band structure calculations to ensure that we correctly infer the strain state of the rolled-up tubes. The optical properties of the light-hole fundamental band gap heterostructures have not been explored yet. In this way, the strain induced by the curved geometry opens an additional way to band-engineer semiconductor nanostructures.

EXPERIMENTAL SECTION

To fabricate rolled-up microtubes (see Figure 1), an initial heterostructure is grown by molecular beam epitaxy (Karl Eberl MBE Komponeten) on a GaAs (100) substrate. For the GaAs-QW sample (Figure 1a), a 40 nm AlAs sacrificial layer was grown followed by a nominal 15 nm $In_{0.2}Ga_{0.8}As$ strained layer, a 20 nm $Al_{0.33}Ga_{0.67}As$ layer, a nominal 4 nm GaAs (QW) layer, a 20 nm $Al_{0.33}Ga_{0.67}As$ layer, and a 5 nm GaAs cap layer. For the InGaAs-QW sample (Figure 1a), we grew on top of a 40 nm AlGaAs sacrificial layer a 20 nm $In_{0.2}Al_{0.2}Ga_{0.6}As$ strained layer, a 10 nm GaAs layer, a nominal 4 nm strained $In_{0.2}Ga_{0.8}As$ (QW) layer, and a 20 nm GaAs heterostructure. The tubes were fabricated following a well-established strategy.[21,28,40] In a sequence of photolithographic steps using samples with a size of 10 × 10 mm, first, the roll-up area with a shallow etching step (Figure 1b) containing ca. 5 × 20 tube structures per sample is defined, followed by the definition of a deep trench for the starting edge and a final selective removal of the AlAs sacrificial layer using HF (Figure 1c).[13,14] For the rolled-up tubes, which form by strain relaxation at the moment of the layer release, we expected tube radii of approximately R = 3.2 μm (GaAs-QW) and R = 2.1 μm (InGaAs-QW).[38,41] Figure 1e shows a light microscopy image of a pad of a processed tube area. One can recognize tubes, shallow etched areas, as well as deep

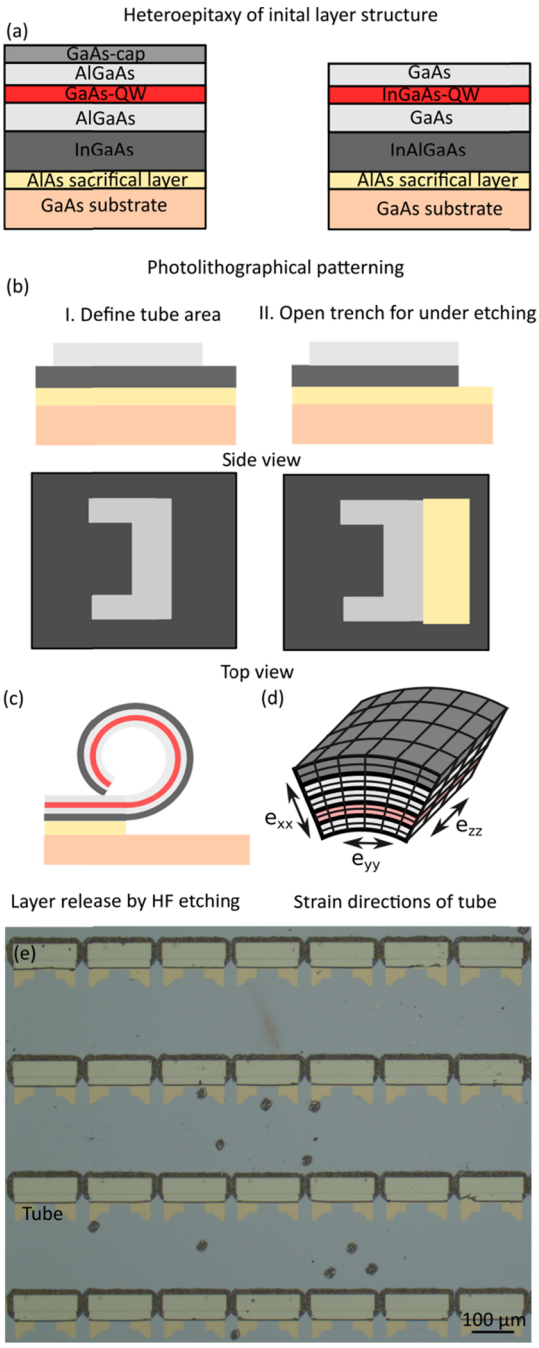

Figure 1. (a) Schematic showing the exact layer structure of the two samples. (b, c) Schematic illustration of the layer structure and the fabrication process. (d) Strain directions as defined inside the tubes (consistent with the directions of the flat layer assuming that the growth direction is the x-direction as required for the simulations). (e) Light microscopy image showing the processed tube area. Tubes are homogeneous and without major defects between single defined fields.

trenches. Tubes appear homogeneous from among each other. The obtained tubes were characterized by scanning electron microscopy (SEM) using an FIE Inspec F50 instrument at 20 keV. The samples are tilted to 55° to increase the contrast and allow us to image the tube openings (see images in Figure 2a,b).

The flat grown layers were structurally characterized by high-resolution X-ray diffraction using a Philips X'Pert instrument equipped with a four-bounce Ge monochromator in the primary beam optics and a curved monochromator before the detector using

https://dx.doi.org/10.1021/acsanm.1c00354
ACS Appl. Nano Mater. 2021, 4, 3140−3147

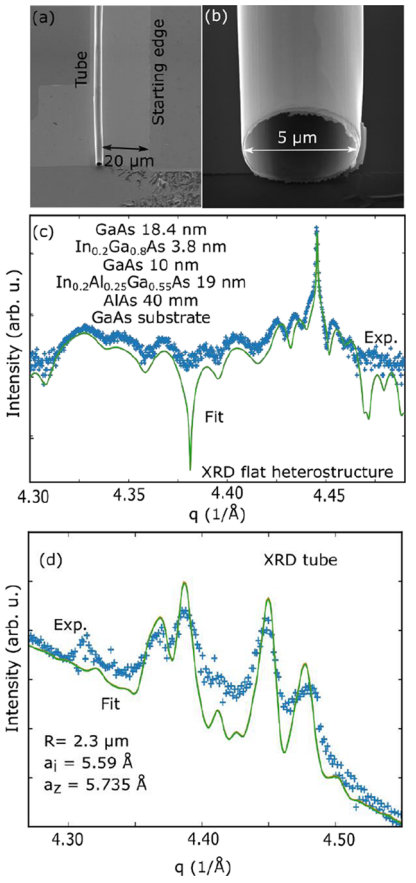

Figure 2. (a, b) SEM images of the GaAs-QW tube. (a) Patterned area and the starting edge of the rolled-up tube. (b) Opening of the tube with ca. 5 μm diameter. (c) XRD measurement and fit of the flat InGaAs-QW sample for determination of the layer thickness and alloy concentrations (provided in the text within the figure panel). (d) XRD pattern and fit of the rolled-up tubes to infer the strain of the rolled-up quantum well.

Cu-kα_1 radiation. The layer thicknesses and alloy concentrations of the initial heterostructure were determined by refining the nominal layer structure using the dynamic diffraction model of the X-ray utility package.[42]

XRD on the tubes was carried out at the XRD2 beamline of the National Brazilian synchrotron laboratory (LNLS) at 9 keV using a 6 + 2 circle diffractometer with a beam footprint covering all tubes on the sample. To obtain a good signal from the tubes, a Pilatus area detector was used with its long axis along the scattering angle path and the samples were detuned from the Bragg conditions, as described before.[38,43] We determined the tubes' inner layer tangential lattice parameter a_i, the tubes longitudinal lattice parameter a_z, and radius R by refining a kinematical diffraction model[36,38,43] against the tubes' diffraction patterns assuming a plane strain state that connects e_{xx} to e_{yy} (given by a_i and R) and e_{zz} (given by a_z).[38,41] The strain state e_{xx} is directly probed by the XRD diffraction experiment. The schematic in Figure 1d provides an overview of the directions of the different strain components (e_{xx}, e_{yy}, and e_{zz}) relative to the tubes' axis (or flat layer directions).

For PL experiments, samples were mounted on a He cold finger cryostat (T = 15 K) and a HeNe laser or a Ti-sapphire laser (Spectra Physics 3900S) under the CW regime was focused using 50× or 100× long-working-distance Mitutoyo objectives down to spot sizes of ca. 2 or 1 μm, respectively, allowing the excitation of a single tube or a nearby flat area. PLE was carried out by tuning the Ti:Sa laser wavelength. Detection was mainly performed with a GaAs photomultiplier (which induces noise for measurements above ~900 nm due to the low quantum efficiency in this range) coupled to a 0.75 m SPEX 1406 double monochromator. Only the spectra in Figure 3 were obtained with an Andor (SR 500) Si-CCD and a single-

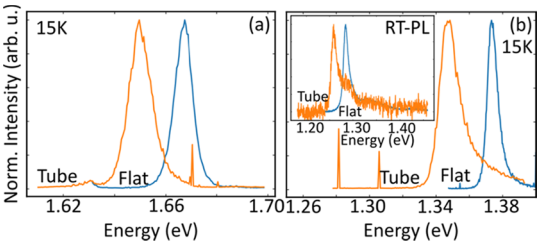

Figure 3. PL spectra of the flat areas and tubes: (a) GaAs-QW (only 15 K) and (b) InGaAs-QW (15 K and room temperature (RT)).

spectrometer system. Fixed circularly polarized incident excitation was used, and the PLE signal was collected for both components of the circular polarizations (σ^+ and σ^-). Pol = $(I^+ - I^-)/(I^+ + I^-)$ is defined as the degree of spin polarization, where the measured PLE intensities are given by I^+ and I^- for σ^+ and σ^- configurations, respectively. We have performed several measurements per sample on different positions on the flat area and rolled-up tubes to ensure good reproducibility. All of them have similar behavior, which we present here.

Band structure, transition energies, and absorption spectra were calculated for flat and rolled-up tubes using the NextNano++ software package for room and low temperatures (15 K). The nominal thicknesses of the QWs were slightly adjusted to match the transition energies observed in PL of the flat layers (3.6 nm for the GaAs-QW and 3.8 nm InGaAs-QW). For the flat layers, a pseudomorphic strain originating from the lattice match to the GaAs substrate is assumed and included by NextNano++. For the rolled-up structures, we implemented a one-dimensional (1D) strain profile in the NextNano input file following the directions layout shown in Figure 1d. As the strain in GaAs-QW samples was previously well investigated,[36] the strain profile of the GaAs-QW as well as for the theoretical investigation was determined for this structure providing R, a_i, and a_z deduced by energy minimization.[38,41] For the InGaAs-QW, R, a_i, and a_z were obtained directly from XRD diffraction on the rolled-up tube ensuring agreement with the μ-PL results.

RESULTS AND DISCUSSION

The SEM image of a rolled-up GaAs-QW tube is depicted in Figure 2a. We can identify the starting edge as well as the defined area for rolling-up. The rolled-up tube is formed 20 μm away from its starting edge, performing more then one rotations on the surface. Figure 2b shows the SEM image of the GaAs-QW tube allowing us to identify layers (windings) forming the tube with a diameter of ca. 5 μm, which is slightly smaller than expected. This indicates that layer thickness might be slightly smaller than the nominal value. The image proves that the tubes form in a tight, well-behaved manner and have no loose windings.

As pointed out before, the exact strain state of a heterostructure depends on its relaxation during roll-up. As our theoretical calculation (see discussion below) for InGaAs-QW predicted drastic changes, we decided to determine the exact strain state of the InGaAs-QW experimentally. Therefore, the XRD pattern in the vicinity of the GaAs (400) peak as a function of scattering vector $q = 4\pi/\lambda \sin(\theta)$, with λ being the wavelength and 2θ being the Bragg angle of the flat heterostructure used for the InGaAs-QW tubes, is provided in Figure 2c. The calculated diffraction curve (solid line) was deduced from the layer structure given in the figure. The XRD fit obtained for this measurement determines that the values for the heterostructure are close to the ones that are used as

https://dx.doi.org/10.1021/acsanm.1c00354
ACS Appl. Nano Mater. 2021, 4, 3140−3147

the InGaAs-QW thickness in the NextNano++ calculations. Figure 2d depicts the experimental XRD diffraction pattern and the fit of the experimental data of an InGaAs-QW tube sample as a function of q. To achieve a good fit, we slightly adjusted the indium concentration (from 0.20 to 0.18) between the planar heterostructure and the rolled-up tubes. This small difference is compatible with experimental uncertainty and inhomogeneity of the MBE growth over the sample size. For the $k{\cdot}p$ calculations, we always used an indium concentration of 0.20 to agree with the observed transition energy measured in PL as well as be consistent with the flat layers. Indeed, the separation of the In(Al)GaAs straining layer and InGaAs-QW in the tube diffraction signal is complicated due to the simplicity of the applied model. On the other hand, the overall strain state is deduced with great certainty as directly determined by the interatomic distances measured by the XRD. Hence, to ensure experimental consistency, strain profiles are taken from the tubes' diffraction, whereas layer thickness and indium content from the flat layer XRD were determined with greater reliability. The XRD of the tubes allows determination of the average tube radius (R = 2.3 μm), a_i = 5.59 Å, and a_z = 5.735 Å, which agrees with the theoretically expected values.

To characterize the optical properties of the rolled-up tubes, we measured the PL spectra and show them in Figure 3. Figure 3a (also in Figure 4a) depicts the normalized PL spectra of the

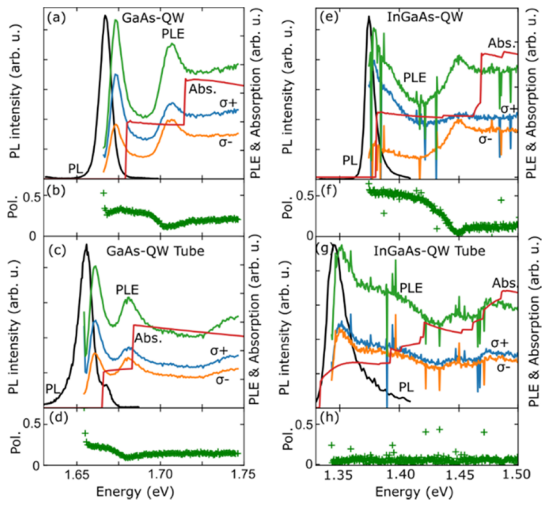

Figure 4. (a) PL (black) and PLE (green is unpolarized, and blue and orange are σ^+ and σ^- polarizations, respectively) spectra of the flat GaAs-QW structure and calculated absorption spectrum (red). (b) Polarization degree of the flat GaAs-QW. (c) PL and PLE spectra of the rolled-up GaAs-QW structure. (d) Polarization degree of the rolled-up GaAs-QW tubes. (e) PL and PLE spectra of the flat InGaAS-QW sample. (f) Polarization degree of the flat InGaAs-QW. (g) PL and PLE of the rolled-up InGaAs-QW. Calculation suggests an inversion of the LH and HH band profiles to obtain the correct transition energies. (h) Polarization degree of the rolled-up InGaAs-QW.

flat unrolled GaAs-QW. We observe a strong PL peak at 1.667 eV originating from the heavy-hole (HH) exciton emission of the GaAs-QW. For the rolled-up GaAs-QW spectrum depicted in Figure 3b (and Figure 4c), we observe a redshift (11 meV) of the ground-state PL emission of the QW to 1.656 eV. This behavior is in agreement with previous results for a rolled-up GaAs-QW.[36]

For the flat InGaAs-QW shown in Figure 3b (included in Figure 4e), we observe a PL peak at 1.374 eV. The rolled-up InGaAs-QW spectrum depicted in Figure 3b (and Figure 4g) displays a PL emission red-shifted by 29 meV to 1.345 eV. It is worth pointing out that we can detect the PL of the InGaAs-QW at room temperature (RT) (shown in the inset of Figure 3b) at 1.283 eV (flat layer) and 1.260 eV (rolled-up tubes) exhibiting an energy shift in the same range of 23 meV, indicating the good quality of the heterostructures. Although for the GaAs-QW, the width of the PL line does not significantly change between tubes and flat layer, the tubes' PL of the InGaAs-QW is relatively broader than the flat layer. We ascribe this to the more complex strain state of the InGaAs-QW.

The low-temperature unpolarized PLE spectra (green solid line) for the flat GaAs-QW are shown in Figure 4a. For convenience, we again plot the PL spectra in the same figure. The PLE spectrum of this flat structure shows typical behavior of QW systems corresponding to the two-dimensional excitonic transitions with two clear peaks at 1.673 and 1.706 eV of heavy-hole (HH) and light-hole (LH) exciton absorption peaks, respectively. The difference between the two peaks is the separation of the confined energy levels of the HH and LH in the flat GaAs-QW (33 meV). The shape of the PLE does not change significantly between flat and rolled-up QWs, but the spectral position of the HH and LH are at lower energies (1.660 and 1.681 eV), respectively. Hence, the HH and LH splitting energy decreases from 33 to 21 meV. Although the PLE is typical for a two-dimensional system (QW), it indicates already a decrease in the separation of the LH and HH states from the flat to the rolled-up structure. For both structures, the calculated absorption (red solid line) is shifted to higher energies, but the energy separation between two excitons is in good agreement with the measured one.

The PLE spectrum of the flat InGaAs-QW (Figure 4e) shows two main peaks at 1.379 and 1.450 eV, which are attributed to HH and LH exciton transitions, respectively. For the rolled-up tubes (Figure 4g), the observed PLE spectrum changes significantly compared to the other ones, which have exhibited the typical form of a quantum well absorption. The spectrum exhibits no clear excitonic-like peak, except for the ground-state transition, at 1.351 eV. Nevertheless, we can observe other broad bands which we ascriebe to transition from continuum states indicating that the electronic structure is drastically changed.

To understand the changes in the PL and PLE spectra for rolled-up QWs, we calculated the band structure of the valence (HH and LH holes, Figure 5) and the conduction bands (not shown) as well as the absorption spectra (red lines in Figure 4). The calculated HH and LH valence (dark red and green line) band edge potential profiles, ground-state confined levels (E_{HH} and E_{LH}), and square module of the ground-state wave function Ψ^2 for the flat 3.6 nm GaAs-QW are shown in Figure 5a. Using the depicted potential profile, which takes the strain tensor elements as determined previously into account, we calculated the absorption spectra shown in Figure 4 (red solid lines). The expected transition energies between the ground state of the HH and LH sub-band to electron sub-band are 1.680 and 1.715 eV, respectively, with an HH−LH splitting energy of 35 meV (in very good agreement with the PLE experimental value of 33 meV). The slight blueshift of the transitions with respect to the exciton absorption edge observed in the PLE measurements is mainly associated with

https://dx.doi.org/10.1021/acsanm.1c00354
ACS Appl. Nano Mater. 2021, 4, 3140−3147

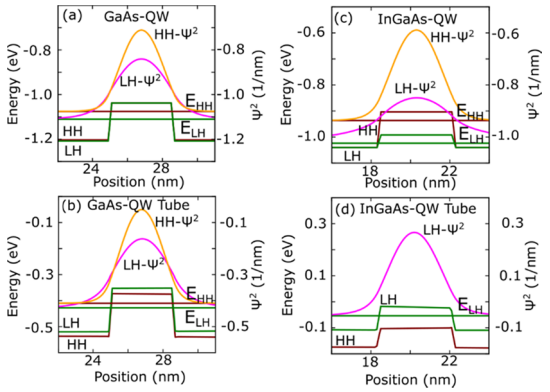

Figure 5. Valence-band potential profiles (green line for LH and dark red for HH) and calculated square of the ground-state wave function for the (a) flat GaAs-QW, (b) rolled-up GaAs-QW, (c) flat InGaAs-QW, and (d) rolled-up InGaAs-QW.

the GaAs-QW exciton binding energy,[44] which is not included in the calculation.

In Figure 5b, the calculated valence-band structure for the rolled-up GaAs-QW is depicted. The corresponding calculated transition energies are 1.667 and 1.682 eV for HH and LH transitions, respectively, and both energies are redshifted (see Figure 4c). However, the redshift of the LH transition is larger than for HH, resulting in a reduction of the HH−LH splitting from 30 to 15 meV, in agreement with the experimental data (33−21 meV). The energy shift is seen clearly in Figure 5b, where the LH potential profile below the HH, but the confined energy level of the LH ground state (E_{LH}), is still above the HH ground-state energy (E_{HH}). This is the first indication that potentially one can invert the HH and LH confinement energy using the strain distribution of a rolled-up tube.

Similar calculations have been carried out for the InGaAs-QW, and the obtained band structure for the flat structure is depicted in Figure 5c. We obtained an HH transition energy of 1.381 eV and an LH transition of 1.460 eV with a HH−LH splitting of 79 meV, slightly larger than the experimental one (71 meV) for the flat structure (Figure 4e). Note that despite the LH transition shows a weak shoulder at 1.464 eV in the absorption spectrum in Figure 4e, its exciton absorption forms a quite defined peak, as observed in the PLE spectrum. The shoulder-like behavior at 1.464 eV in the absorption spectrum reflects the fact that we no longer have a completely parabolic dispersion due to asymmetry of the InGaAs-QW. Above the LH transition ground state, we have delocalized states and absorption related to the barrier states, which are not probed in the PLE experiment. The small absorption at 1.437 eV can be identified as a transition corresponding to second heavy-hole-state exciton transition (forbidden transition). The asymmetry of InGaAs-QW can induce the breaking of the selection rule optical transitions for quantum wells.

Unlike the GaAs-QW, the band structure calculated for the rolled-up InGaAs-QW undergoes significant changes, as seen in Figure 5d. Our calculations indicate an inversion of the LH and HH potential profiles. Moreover, the bottom of the HH potential profile coincides approximately with the barrier of the LH profile and we find therefore continuous states of the LH in resonance with the HH sub-bands in the quantum well, as shown in Figure 5d. For this potential profile, therefore, only one confined bound state is found in the valence band, which is the LH sub-band with a transition energy of ca. 1.333 eV (slightly smaller than that observed in PLE). Interestingly, our calculation underestimates the transition energy compared to calculations for the GaAs-QW and the flat InGaAs heterostructure. This is ascribed to the rather unique strain state of the InGaAs-QW, where strain relaxation is determined by two straining layers (InGaAs-QW and the bottom InAlGaAs layer). Furthermore, there are strong admixes between delocalized HH and LH functions, implying transitions between the continuum of states at higher energies for this sample. Therefore, we cannot identify transitions above the LH ground state. These states reflect a broad transition around 1.40 eV in PLE spectra due to several wavefunctions overlaps that we cannot resolve in the experimental data. This effect emerges from the strong asymmetric strain in the InGaAs-QW caused by the roll-up. This strain profile results in the tilted potential profile of HH and LH sub-bands.

This fundamental change in the band structure is reflected in the experimental result as well as in the calculated absorption spectrum seen in Figure 4g. The absorption becomes a continuum line without any typical steps observed for the other structures in good agreement with the experimental data (green line in Figure 4g). To demonstrate how profound the changes in the electronic structure are, we tested the selection rules of the optical transitions by carrying out circularly polarized PLE measurements.

In Figure 4a, we depict the circular polarization-dependent PLE signal of the flat GaAs-QW. The two components of the PLE spectra (σ^+ and σ^-) show both HH and LH exciton peaks, as observed in the unpolarized spectra in Figure 4a. The degree of emitted circular polarization is shown in Figure 4b. For excitation near the resonance with the HH exciton transition, the polarization degree is ca. 30%. Increasing the excitation energy, a clear dip is observed at the position of the LH exciton peak in the PLE spectrum. The optical selection rules for absorption in the HH and LH states in GaAs-QWs predict photocreated electrons with opposite spin orientation for each case. This is a fingerprint allowing identification of transitions involving the LH sub-band by the presence of the dip in polarization-resolved PLE spectrum.[45]

For the rolled-up GaAs-QW, the polarization-dependent PLE spectra (Figure 4c) and the spin polarization degree (Figure 4d) are very similar to those for the flat GaAs-QW. The main difference is the redshift of all peaks and smaller HH−LH energy splitting of this structure, as expected theoretically. Once more, the clear dip in the polarization degree shows unambiguously the nature of the LH exciton transition.

Similarly, we analyzed the polarization dependence of the PLE in the InGaAs-QW, which is depicted in Figure 4e. In this structure, we observe a larger polarization degree close to the HH absorption (~60%) for the flat layer (Figure 4f). The overall behavior of the spin polarization curve is similar to the one observed for the GaAs-QW, with a strong reduction of the polarization degree at the LH absorption edge.

In contrast to the previous cases, the degree of spin polarization in the rolled-up InGaAs-QW shows a dramatically different behavior (see Figure 4g,h). In this case, the polarization degree is negligible in the entire energy range. This change is ascribed to the strong mixing between the HH and LH valence bands, resulting in a drastic change in the spin selection rules.

To understand if our findings are general for all InGaAs-QW integrated into a tube with different diameters, we theoretically

https://dx.doi.org/10.1021/acsanm.1c00354
ACS Appl. Nano Mater. 2021, 4, 3140−3147

investigate the influence of the asymmetric strain on the InGaAs-QW emission. Therefore, we increase the curvature of our structure by systematically changing the indium content in the first In(Al)GaAs layer. The strain-dependent shift of the light-hole (LH)−electron (e) and heavy-hole (HH)−electron (e) transitions between valence and conduction bands at the Γ point in III−V materials is well investigated for a biaxial strain state. Rolled-up tubes form a different strain state that depends on how the tubes relax as well as on the thickness of the initial heterostructure. In the literature, one can find analytical solutions for a plain stress, plain strain, and intermediate states.[35,41,46−48] We assume a plain strain state (as it has shown experimentally a good description for the system investigated here[39]) and carry out energy minimization calculations to find the R, a_i, and a_z for a given indium content. Hereby, it is worth pointing out that with increasing indium content, the R and a_i values will decrease, but a_z will increase, giving rise to an asymmetric strain state.

Figure 6 shows the result of the NextNano calculation for a rolled-up GaAs-QW and InGaAs-QW embedded into a tube

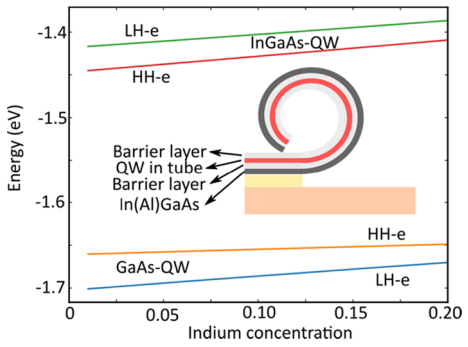

Figure 6. Calculated transition energies of the rolled-up GaAs-QW and InGaAs-QW varying the indium content of the straining layer and, hence, the radius and the inner and outer lattice parameters of the tubes. With increasing indium content (decreasing R and a_i, and increasing a_z), we observe a systematic shift of the LH−e and HH−e transitions to smaller energies. Interestingly, for the InGaAs-QW, the LH and HH states invert as soon as the original epi-structure is released and forms a tube.

wall, which has relaxed to the energetic minimum (which is not the case for the real sample of InGaAs-QW). The indium content of the straining layer was changed from 0.01 to 0.2, and the HH−e and LH−e transitions were calculated for each value of R, a_i, and a_z.

For the GaAs-QW the HH−e transition is always above the LH−e transition, but due to the triaxial strain state with decreasing radius (increasing indium content), the separation of the LH and HH transition decreases. We observe a crossing of the band edges, but due to the different hole masses, the HH state is always above the LH state. Interestingly, for the InGaAs-QW, any relaxation of the epi-layers into the triaxial strain state of the tubes results in an inversion of the LH and HH states, and hence the LH−e transition should be below the HH−e transition in energy. However, unlike the GaAs-QW, the separation of the two transitions remains constant (or quasi-constant) and shifts systematically to lower energies for smaller radii (higher indium content). This should result from the different material parameters of the indium alloy and the unusual strain state of the tubes.

Despite the calculated ground state of the QW showing an LH exciton transition, this is a mixed state due to the anti-crossing effects that admixes the HH and LH bands as seen by our polarization-sensitive PLE measurements. Therefore, even under near-resonance excitation, the degree of spin polarization of the emitted light is negligible. This has been observed in all tubes investigated despite small variations in PLE spectra indicating small fluctuations in the strain state. This is a confirmation that the curvature-induced strain state changes fundamentally the band structure of the rolled-up tubes. As we have full control of the curvature by the initial design of the heterostructure,[35] we can use it to band-engineer the optical properties of the integrated quantum emitter and use them, for example, as unpolarized light sources.

CONCLUSIONS

In conclusion, we investigated the effects of geometrically induced strain on the band structure of III−V semiconductor nanostructures. We demonstrated that the GaAs and InGaAs quantum wells, when simply rolled up, forming tubes, drastically change the band structure and, consequently, their optical properties. The tubes were designed to move heavy- and light-hole sub-bands toward each other to achieve the crossing and increase the band mixing effects. These effects were clearly observed using circularly polarized PLE. As rolled-up tubes have also been used as optical cavities and laser devices,[21,28] the effects of the band mixing between the HH and LH sub-bands are an alternative way to fabricate semiconductor lasers with different emission properties. Similarly, this method can be applicable for other nanometric quantum emitters, e.g., to switch the ground-state emission of a quantum dot.[7,8] In addition, we would like to emphasize that the optical properties behavior presented as a result of the GaAs- and InGaAs-QW nanostructure embedded in the curved system can be used as a model for other physical systems. The effect observed here can be very promising for basic studies of the optical properties and band structure for tensile-strained Ge films[2−4] and different quantum heterostructures.[6−12] Moreover, as we have a tensile and compressive hybrid state that leads to changes in the band potential profile (confinement potential), such an approach can also be applied to other fundamental studies as quantum-confined strain gradient effect.[49] Besides the interest for the quantum information technology in the switching and control of the excitonic states,[50] spin splitting effects originated from interface-induced mixing of valence-band states[51] can be explored.

AUTHOR INFORMATION

Corresponding Author

Christoph Deneke − *Instituto de Física "Gleb Wataghin", Universidade Estadual de Campinas (Unicamp), 13083-859 Campinas, SP, Brazil;* orcid.org/0000-0002-8556-386X; Email: cdeneke@ifi.unicamp.br

Authors

Leonarde N. Rodrigues − *Laboratório Nacional de Nanotecnologia (LNNano), Centro Nacional de Pesquisa em Energia e Materiais (CNPEM), 13083-970 Campinas, SP, Brazil; Departamento de Física, Universidade Federal de Viçosa (UFV), 36570-000 Viçosa, MG, Brazil;* orcid.org/0000-0002-1992-5754

https://dx.doi.org/10.1021/acsanm.1c00354
ACS Appl. Nano Mater. 2021, 4, 3140−3147

Diego Scolfaro − *Instituto de Física "Gleb Wataghin", Universidade Estadual de Campinas (Unicamp), 13083-859 Campinas, SP, Brazil*
Lucas da Conceição − *Laboratório Nacional de Nanotecnologia (LNNano), Centro Nacional de Pesquisa em Energia e Materiais (CNPEM), 13083-970 Campinas, SP, Brazil; Instituto de Física "Gleb Wataghin", Universidade Estadual de Campinas (Unicamp), 13083-859 Campinas, SP, Brazil*
Angelo Malachias − *Departamento de Física, Universidade Federal de Minas Gerais, 31270-901 Belo Horizonte, MG, Brazil*
Odilon D. D. Couto, Jr − *Instituto de Física "Gleb Wataghin", Universidade Estadual de Campinas (Unicamp), 13083-859 Campinas, SP, Brazil*
Fernando Iikawa − *Instituto de Física "Gleb Wataghin", Universidade Estadual de Campinas (Unicamp), 13083-859 Campinas, SP, Brazil*

Complete contact information is available at: https://pubs.acs.org/10.1021/acsanm.1c00354

Author Contributions

L.N.R., D.S., O.D.D.C., and F.I. carried out the optical measurements and provide input for the interpretation. L.d.C. and C.D. grew the samples. L.d.C. and L.N.R. processed the samples. C.D. and A.M. carried out the XRD. C.D. carried out the SEM and the NextNano calculations with input from L.N.R., O.D.D.C., and F.I.; designed the experiment; and supervised the work. The manuscript was written through contributions of all authors. All authors have given approval to the final version of the manuscript.

Funding

The research was supported by FAPESP (2016/14001-7, 2012/11382-9) and CNPq (42392/2016, 432882/2018-9, 162576/2017-0, 306107/2019-8, and 306107/2019-8).

Notes

The authors declare no competing financial interest.

■ ACKNOWLEDGMENTS

The authors acknowledge access to the MBE facilities of the LNNano/CNPEM as well as beamtime granted by the LNLS. The help of Davi Henrique S. de Camargo and Cesar Bof Bufon during sample processing in the LNNano cleanroom facilities is acknowledged. The authors thank LNNano for granting access to the SEM facility.

■ ABBREVIATIONS

InGaAs-QW, InGaAs quantum well
GaAs-QW, GaAs quantum well
QW, quantum well
μ-PL, micro-photoluminescence
μ-PLE, micro-photoluminescence excitation
XRD, X-ray diffraction
HH, heavy hole
LH, light hole
RT, room temperature

■ REFERENCES

(1) Flachowsky, S.; Wei, A.; Illgen, R.; Herrmann, T.; Höntschel, J.; Horstmann, M.; Klix, W.; Stenzel, R. Understanding Strain-Induced Drive-Current Enhancement in Strained-Silicon n-MOSFET and p-MOSFET. *IEEE Trans. Electron Devices* **2010**, *57*, 1343−1354.
(2) Vitiello, E.; Virgilio, M.; Giorgioni, A.; Frigerio, J.; Gatti, E.; De Cesari, S.; Bonera, E.; Grilli, E.; Isella, G.; Pezzoli, F. Spin-Dependent Direct Gap Emission in Tensile-Strained Ge Films on Si Substrates. *Phys. Rev. B* **2015**, *92*, No. 201203.
(3) Giorgioni, A.; Pezzoli, F.; Gatti, E.; Cecchi, S.; Kazuo Inoki, C.; Deneke, C.; Grilli, E.; Isella, G.; Guzzi, M. Optical Tailoring of Carrier Spin Polarization in Ge/SiGe Multiple Quantum Wells. *Appl. Phys. Lett.* **2013**, *102*, No. 012408.
(4) Sánchez-Pérez, J. R.; Boztug, C.; Chen, F.; Sudradjat, F. F.; Paskiewicz, D. M.; Jacobson, R.; Lagally, M. G.; Paiella, R. Direct-Bandgap Light-Emitting Germanium in Tensilely Strained Nanomembranes. *Proc. Natl. Acad. Sci. U.S.A.* **2011**, *108*, 18893−18898.
(5) Ning, C.-Z.; Dou, L.; Yang, P. Bandgap Engineering in Semiconductor Alloy Nanomaterials with Widely Tunable Compositions. *Nat. Rev. Mater.* **2017**, *2*, 1−14.
(6) Rastelli, A.; Ding, F.; Plumhof, J. D.; Kumar, S.; Trotta, R.; Deneke, C.; Malachias, A.; Atkinson, P.; Zallo, E.; Zander, T.; Herklotz, A.; Singh, R.; Krapek, V.; Schroeter, J. R.; Kiravittaya, S.; Benyoucef, M.; Hafenbrak, R.; Joens, K. D.; Thurmer, D. J.; Grimm, D.; Bester, G.; Doerr, K.; Michler, P.; Schmidt, O. G. Controlling Quantum Dot Emission by Integration of Semiconductor Nanomembranes onto Piezoelectric Actuators. *Phys. Status Solidi B* **2012**, *249*, 687−696.
(7) Huo, Y. H.; Witek, B. J.; Kumar, S.; Cardenas, J. R.; Zhang, J. X.; Akopian, N.; Singh, R.; Zallo, E.; Grifone, R.; Kriegner, D.; Trotta, R.; Ding, F.; Stangl, J.; Zwiller, V.; Bester, G.; Rastelli, A.; Schmidt, O. G. A Light-Hole Exciton in a Quantum Dot. *Nat. Phys.* **2014**, *10*, 46−51.
(8) Zhang, J.; Huo, Y.; Rastelli, A.; Zopf, M.; Höfer, B.; Chen, Y.; Ding, F.; Schmidt, O. G. Single Photons On-Demand from Light-Hole Excitons in Strain-Engineered Quantum Dots. *Nano Lett.* **2015**, *15*, 422−427.
(9) Huo, Y. H.; Rastelli, A.; Schmidt, O. G. Ultra-Small Excitonic Fine Structure Splitting in Highly Symmetric Quantum Dots on GaAs (001) Substrate. *Appl. Phys. Lett.* **2013**, *102*, No. 152105.
(10) Wang, X.; Cui, X.; Bhat, A.; Savage, D. E.; Reno, J. L.; Lagally, M. G.; Paiella, R. Ultrawide Strain-Tuning of Light Emission from InGaAs Nanomembranes. *Appl. Phys. Lett.* **2018**, *113*, No. 201105.
(11) Wang, J.; Yin, Y.; Hao, Q.; Huang, S.; Saei Ghareh Naz, E.; Schmidt, O. G.; Ma, L. External Strain Enabled Post-Modification of Nanomembrane-Based Optical Microtube Cavities. *ACS Photonics* **2018**, *5*, 2060−2067.
(12) Trotta, R.; Atkinson, P.; Plumhof, J. D.; Zallo, E.; Rezaev, R. O.; Kumar, S.; Baunack, S.; Schröter, J. R.; Rastelli, A.; Schmidt, O. G. Nanomembrane Quantum-Light-Emitting Diodes Integrated onto Piezoelectric Actuators. *Adv. Mater.* **2012**, *24*, 2668−2672.
(13) Prinz, V. Y.; Seleznev, V. A.; Gutakovsky, A. K.; Chehovskiy, A. V.; Preobrazhenskii, V. V.; Putyato, M. A.; Gavrilova, L. A. Free-Standing and Overgrown InGaAs/GaAs Nanotubes: Fabrication, Potential Applications. *Phys. E* **2000**, *6* (1−4), 828−831.
(14) Schmidt, O. G.; Schmarje, N.; Deneke, C.; Muller, C.; Jin-Phillipp, N. Y. Three-Dimensional Nano-Objects Evolving from a Two-Dimensional Layer Technology. *Adv. Mater.* **2001**, *13*, 756−759.
(15) Deneke, C.; Songmuang, R.; Jin-Phillipp, N. Y.; Schmidt, O. G. The Structure of Hybrid Radial Superlattices. *J. Phys. D: Appl. Phys.* **2009**, *42*, No. 103001.
(16) Cho, A. New Trick with Silicon Film Could Herald a Bright Future for Rolled-up Nanotubes. *Science* **2006**, *311*, 1861.
(17) Schmidt, O. G.; Deneke, C.; Kiravittaya, S.; Songmuang, R.; Heidemeyer, H.; Nakamura, Y.; Zapf-Gottwick, R.; Muller, C.; Jin-Phillipp, N. Y. Self-Assembled Nanoholes, Lateral Quantum-Dot Molecules, and Rolled-up Nanotubes. *IEEE J. Sel. Top. Quantum Electron.* **2002**, *8*, 1025−1034.
(18) Moradi, S.; Naz, E. S. G.; Li, G.; Bandari, N.; Bandari, V. K.; Zhu, F.; Wendrock, H.; Schmidt, O. G. Highly Symmetric and Extremely Compact Multiple Winding Microtubes by a Dry Rolling Mechanism. *Adv. Mater. Interfaces* **2020**, *7*, No. 1902048.
(19) Barcelos, I. D.; Marçal, L. A. B.; Deneke, C.; Moura, L. G.; Lacerda, R. G.; Malachias, A. Direct Evaluation of CVD Multilayer Graphene Elastic Properties. *RSC Adv.* **2016**, *6*, 103707−103713.

(20) Schulz, K. M.; Vu, H.; Schwaiger, S.; Rottler, A.; Korn, T.; Sonnenberg, D.; Kipp, T.; Mendach, S. Controlling the Spontaneous Emission Rate of Quantum Wells in Rolled-Up Hyperbolic Metamaterials. *Phys. Rev. Lett.* **2016**, *117*, No. 085503.
(21) Kipp, T.; Welsch, H.; Strelow, C.; Heyn, C.; Heitmann, D. Optical Modes in Semiconductor Microtube Ring Resonators. *Phys. Rev. Lett.* **2006**, *96*, No. 077403.
(22) Kipp, T.; Strelow, C.; Welsch, H.; Heyn, C.; Heitmann, D. In *Optical Microtube Ring Resonators*, AIP Conference Proceedings; American Institute of Physics, 2007; pp 1127−1128.
(23) Strelow, C.; Rehberg, H.; Schultz, C. M.; Welsch, H.; Heyn, C.; Heitmann, D.; Kipp, T. Optical Microcavities Formed by Semiconductor Microtubes Using a Bottlelike Geometry. *Phys. Rev. Lett.* **2008**, *101*, No. 127403.
(24) Hosoda, M.; Kishimoto, Y.; Sato, M.; Nashima, S.; Kubota, K.; Saravanan, S.; Vaccaro, P. O.; Aida, T.; Ohtani, N. Quantum-Well Microtube Constructed from a Freestanding Thin Quantum-Well Layer. *Appl. Phys. Lett.* **2003**, *83*, 1017−1019.
(25) Huang, G. S.; Kiravittaya, S.; Quinones, V. A. B.; Ding, F.; Benyoucef, M.; Rastelli, A.; Mei, Y. F.; Schmidt, O. G. Optical Properties of Rolled-up Tubular Microcavities from Shaped Nanomembranes. *Appl. Phys. Lett.* **2009**, *94*, No. 141901.
(26) Songmuang, R.; Rastelli, A.; Mendach, S.; Deneke, C.; Schmidt, O. G. From Rolled-up Si Microtubes to SiOx/Si Optical Ring Resonators. *Microelectron. Eng.* **2007**, *84*, 1427−1430.
(27) Wang, J.; Yin, Y.; Yang, Y.-D.; Hao, Q.; Tang, M.; Wang, X.; Saggau, C. N.; Karnaushenko, D.; Yan, X.; Huang, Y.-Z.; Ma, L.; Schmidt, O. G. Deterministic Yet Flexible Directional Light Emission from Spiral Nanomembrane Cavities. *ACS Photonics* **2019**, *6*, 2537−2544.
(28) Li, F.; Mi, Z. T. Optically Pumped Rolled-up InGaAs/GaAs Quantum Dot Microtube Lasers. *Opt. Express* **2009**, *17*, 19933−19939.
(29) Yang, S.; Wang, Y.; Sun, H. Advances and Prospects for Whispering Gallery Mode Microcavities. *Adv. Opt. Mater.* **2015**, *3*, 1136−1162.
(30) Chen, X. An Analytical Model to Investigate the Resonant Modes of the Self-Rolled-up Microtube Using Conformal Transformation. *Opt. Express* **2014**, *22*, 16363−16376.
(31) Chai, Z.; Wang, Q.; Cao, J.; Mao, G.; Liu, H.; Ren, X.; Maleev, N. A.; Vasil'ev, A. P.; Zhukov, A. E.; Ustinov, V. M. Optically Pumped Lasing in a Rolled-up Dot-in-a-Well (DWELL) Microtube via the Support of Au Pad. *Appl. Phys. B* **2018**, *124*, 21.
(32) Hosoda, M.; Shigaki, T. Degeneracy Breaking of Optical Resonance Modes in Rolled-up Spiral Microtubes. *Appl. Phys. Lett.* **2007**, *90*, No. 181107.
(33) Mendach, S.; Songmuang, R.; Kiravittaya, S.; Rastelli, A.; Benyoucef, M.; Schmidt, O. G. Light Emission and Wave Guiding of Quantum Dots in a Tube. *Appl. Phys. Lett.* **2006**, *88*, No. 111120.
(34) Mendach, S.; Kiravittaya, S.; Rastelli, A.; Benyoucef, M.; Songmuang, R.; Schmidt, O. G. Bidirectional Wavelength Tuning of Individual Semiconductor Quantum Dots in a Flexible Rolled-up Microtube. *Phys. Rev. B* **2008**, *78*, No. 035317.
(35) Deneke, C.; Muller, C.; Jin-Phillipp, N. Y.; Schmidt, O. G. Diameter Scalability of Rolled-up In(Ga)As/GaAs Nanotubes. *Semicond. Sci. Technol.* **2002**, *17*, 1278−1281.
(36) Deneke, C.; Malachias, A.; Kiravittaya, S.; Benyoucef, M.; Metzger, T. H.; Schmidt, O. G. Strain States in a Quantum Well Embedded into a Rolled-up Microtube: X-Ray and Photoluminescene Studies. *Appl. Phys. Lett.* **2010**, *96*, No. 143101.
(37) Zhen, H. L.; Huang, G. S.; Kiravittaya, S.; Li, S. L.; Deneke, C. H.; Thurmer, D. J.; Mei, Y. F.; Schmidt, O. G.; Lu, W. Light-Emitting Properties of a Strain-Tuned Microtube Containing Coupled Quantum Wells. *Appl. Phys. Lett.* **2013**, *102*, No. 041109.
(38) Malachias, A.; Deneke, Ch.; Krause, B.; Mocuta, C.; Kiravittaya, S.; Metzger, T. H.; Schmidt, O. G. Direct Strain and Elastic Energy Evaluation in Rolled-up Semiconductor Tubes by x-Ray Microdiffraction. *Phys. Rev. B* **2009**, *79*, No. 035301.
(39) Deneke, C.; Schmidt, O. G. Structural Characterization and Potential X-Ray Waveguiding of a Small Rolled-up Nanotube with a Large Number of Windings. *Appl. Phys. Lett.* **2006**, *89*, No. 123121.
(40) Vorob'ev, A. B.; Prinz, V. Y. Directional Rolling of Strained Heterofilms. *Semicond. Sci. Technol.* **2002**, *17*, 614−616.
(41) Grundmann, M. Nanoscroll Formation from Strained Layer Heterostructures. *Appl. Phys. Lett.* **2003**, *83*, 2444−2446.
(42) Kriegner, D.; Wintersberger, E.; Stangl, J. Xrayutilities: A Versatile Tool for Reciprocal Space Conversion of Scattering Data Recorded with Linear and Area Detectors. *J. Appl. Crystallogr.* **2013**, *46*, 1162−1170.
(43) Deneke, C.; Wild, E.; Boldyreva, K.; Baunack, S.; Cendula, P.; Mönch, I.; Simon, M.; Malachias, A.; Dörr, K.; Schmidt, O. G. Rolled-up Tubes and Cantilevers by Releasing SrRuO3-Pr0.7Ca0.3MnO3 Nanomembranes. *Nanoscale Res. Lett.* **2011**, *6*, 621.
(44) Nelson, D. F.; Miller, R. C.; Tu, C. W.; Sputz, S. K. Exciton Binding Energies from an Envelope-Function Analysis of Data on Narrow Quantum Wells of Integral Monolayer Widths in ${\mathrm{Al}}_{0.4}$${\mathrm{Ga}}_{0.6}$As/GaAs. *Phys. Rev. B* **1987**, *36*, 8063−8070.
(45) Pfalz, S.; Winkler, R.; Nowitzki, T.; Reuter, D.; Wieck, A. D.; Hägele, D.; Oestreich, M. Optical Orientation of Electron Spins in GaAs Quantum Wells. *Phys. Rev. B* **2005**, *71*, No. 165305.
(46) Hsueh, C.-H. Modeling of Elastic Deformation of Multilayers Due to Residual Stresses and External Bending. *J. Appl. Phys.* **2002**, *91*, 9652−9656.
(47) Nikishkov, G. P. Curvature Estimation for Multilayer Hinged Structures with Initial Strains. *J. Appl. Phys.* **2003**, *94*, 5333−5336.
(48) Vaccaro, P. O.; Kubota, K.; Aida, T. Strain-Driven Self-Positioning of Micromachined Structures. *Appl. Phys. Lett.* **2001**, *78*, 2852−2854.
(49) Binder, R.; Gu, B.; Kwong, N. H. Quantum-Confined Strain Gradient Effect in Semiconductor Nanomembranes. *Phys. Rev. B* **2014**, *90*, No. 195208.
(50) Éthier-Majcher, G.; St-Jean, P.; Francoeur, S. Energy Reversal of Light- and Heavy-Hole Excitons Bound to Isoelectronic Centers. *Phys. Rev. B* **2018**, *98*, No. 115431.
(51) Durnev, M. V.; Glazov, M. M.; Ivchenko, E. L. Spin-Orbit Splitting of Valence Subbands in Semiconductor Nanostructures. *Phys. Rev. B* **2014**, *89*, No. 075430.

https://dx.doi.org/10.1021/acsanm.1c00354
ACS Appl. Nano Mater. 2021, 4, 3140−3147